J Oceanogr (2015) 71:449–461
DOI 10.1007/s10872-015-0304-6

ORIGINAL ARTICLE

Mass-induced sea level variations in the Gulf of Carpentaria

Juan Wang[1,2] · Jing Wang[1] · Xuhua Cheng[2]

Received: 10 February 2015 / Revised: 27 May 2015 / Accepted: 31 May 2015 / Published online: 16 June 2015

Abstract In this work, variations in mass-induced sea surface height (SSH_{mass}, ocean bottom pressure) in the Gulf of Carpentaria are investigated on seasonal to decadal timescales using altimetry data, Gravity Recovery and Climate Experiment (GRACE) estimates, and steric sea surface height measurements derived from subsurface temperature and salinity analyses. Seasonal variability in gulf-mean SSH_{mass} can be attributed to local wind forcing. On an interannual and decadal timescale, SSH_{mass} is the dominant factor affecting total sea surface height, and is related to large-scale modes such as the El Niño Southern Oscillation (ENSO) and Pacific Decadal Oscillation (PDO). Oceanic waves propagating from the western Pacific and the corresponding water exchange between the deep ocean and the shallow Gulf of Carpentaria, rather than local wind variability associated with climate modes, are responsible for the low-frequency variations in SSH_{mass} in the gulf. Over 2003–2011, SSH_{mass} rose at a rate of about 8.0 ± 1.5 mm/year, and the PDO accounted for about 65 % of gulf-scale mass variation.

Keywords Mass-induced sea surface height · Steric sea surface height · Sea surface height · ENSO · PDO · GRACE · Gulf of Carpentaria

✉ Jing Wang
jwang@scsio.ac.cn

[1] Guangdong Provincial Key Laboratory of Urbanization and Geo-simulation, School of Geography and Planning, Sun Yat-sen University, 135 West Xingang Road, Guangzhou 510275, China

[2] State Key Laboratory of Tropical Oceanography, South China Sea Institute of Oceanology, Chinese Academy of Sciences, Guangzhou, China

1 Introduction

A rise in sea surface height (SSH) has a potentially devastating impact on coastal societies, resulting in flooding, coastal erosion, salinization of surface and ground waters, and degradation of coastal wetlands habitats (Nicholls 2011). Variations in SSH are largely the result of two processes: one involves steric variations (henceforth denoted as SSH_{steric}) due to changes in temperature and salinity, and the other involves changes in water mass (henceforth denoted as SSH_{mass}) as a result of either ocean mass redistribution or water mass flux (Cazenave and Nerem 2004; Carton et al. 2005; Chambers 2006; Calafat et al. 2010). Altimetry-based estimates of global SSH beginning in1993 have provided a means of measuring the combined effects of steric and mass variation. Objective analysis and ocean data assimilation allow the steric component to be examined alone (Carton et al. 2005; Ishii et al. 2006). Since 2002, the Gravity Recovery and Climate Experiment (GRACE) mission has provided an independent tool to monitor water mass change in the ocean (Nerem et al. 2003; Wahr et al. 2004).

Low-frequency fluctuations in SSH_{mass} (Fig. 1) are strong in the Southern Ocean, North Pacific and semi-enclosed areas at various latitudes (e.g., Indonesian seas, Mediterranean Sea), where the correlation between ocean bottom pressure and SSH is significant (Piecuch et al. 2013). SSH_{mass} variability in the Southern Ocean and North Pacific are mainly driven by changes in wind stress curl (Boening et al. 2011; Cheng et al. 2013). In addition to the GRACE studies in the open ocean, several works have focused on the annual SSH_{mass} cycle in shallow waters such as the Mediterranean Sea, the Gulf of Thailand, and the South China Sea (García et al. 2006; Wouters and Chambers 2010; Cheng and Qi 2010).

Strong variations in SSH_{mass} are present in the Gulf of Carpentaria (hereinafter referred to as the GOC) (Fig. 1). The GOC is enclosed on three sides by northern Australia and bounded on the north by the Arafura Sea. It comprises a water area of approximately 300,000 km^2, with a general depth of between 55 and 66 m and a maximum depth of 82 m (Fig. 2). This gulf features a multi-million-dollar prawn industry—the most valuable prawn industry managed by the Australian government (McLoughlin 2004)—as well as onshore mineral resources including bauxite,

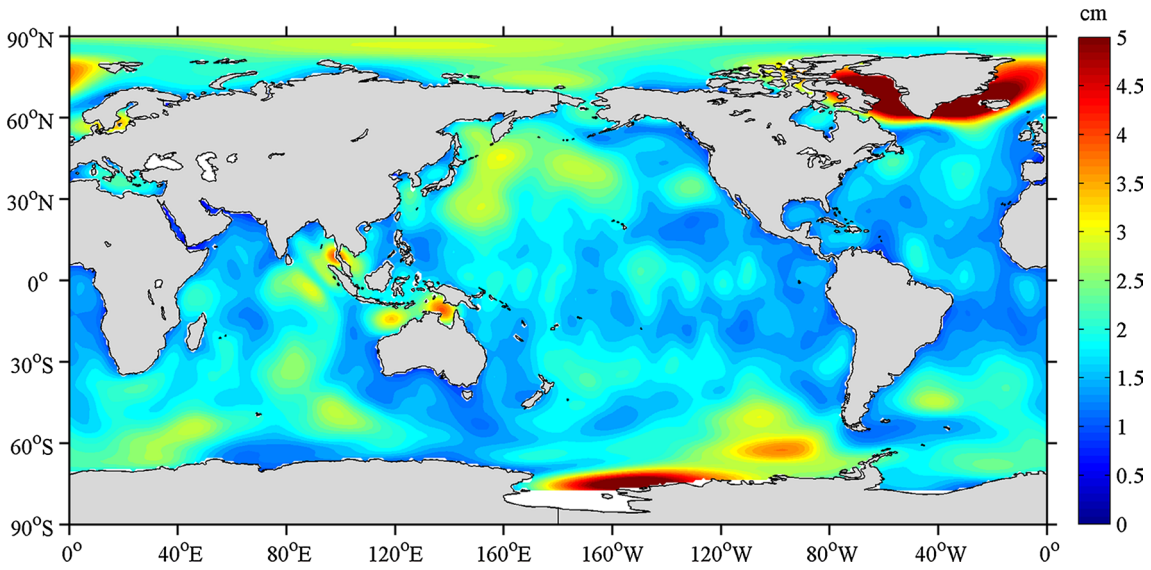

Fig. 1 Standard deviation of SSH_{mass} (cm) derived from GRACE over the period 2003–2011, with its annual cycle removed

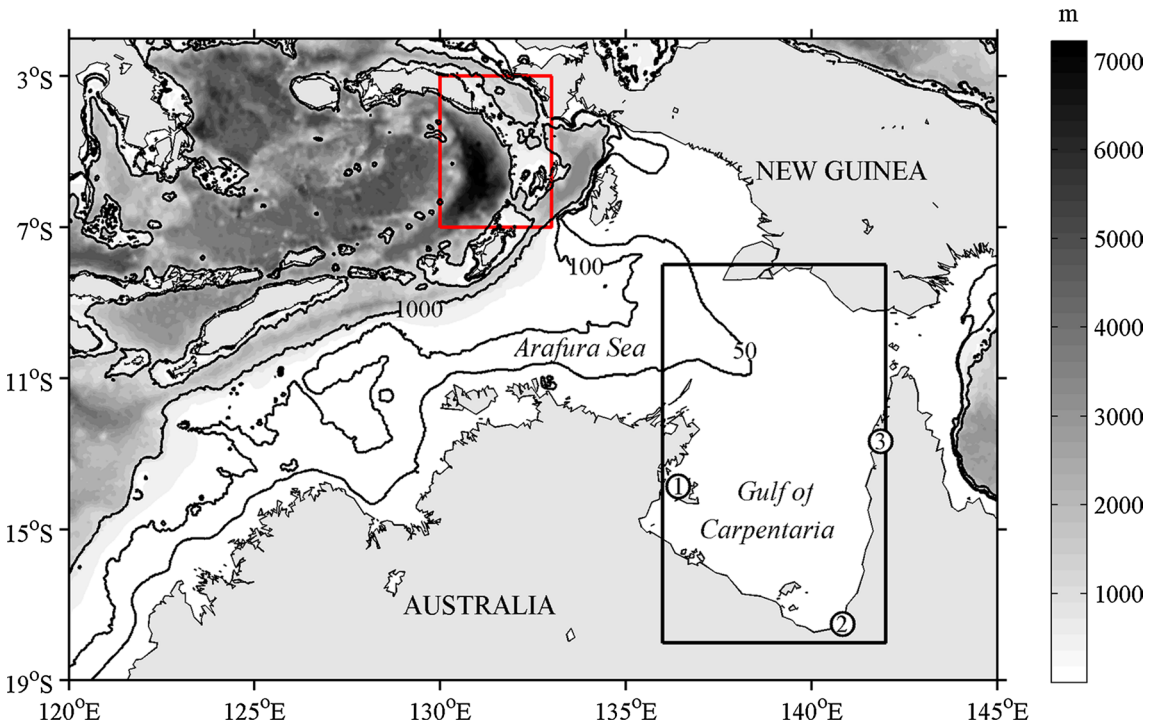

Fig. 2 Bathymetry in Gulf of Carpentaria. The *white circles* show the tide gauge locations: (*1*) Groote Eylandt, (*2*) Karumba, and (*3*) Weipa. The *black box* over the Gulf of Carpentaria encloses the area of interest (136°E–142°E, 18°S–8°S) used to calculate the gulf-mean signal, and the *red box* denotes the area chosen to calculate offshore SSH_{steric}

silver and manganese, and unique ecosystems that include submerged reefs supporting diverse coral communities (Harris 2007). As such, understanding the variations in SSH here may be important for the sustainable management of this region. From a scientific perspective, investigating the features of SSH variations in the GOC and related mechanisms will help to improve our knowledge of how the regional ocean responds to large-scale climate modes such as the El Niño-Southern Oscillation (ENSO) and Pacific Decadal Oscillation (PDO).

Several studies have investigated SSH variations in the GOC. For example, Forbes and Church (1983) studied annual SSH variations in the GOC based on observations of current and SSH from sea bed drifters and buoys. The largest annual range of monthly mean sea level estimates in the GOC is 75 cm, in the southeast corner, and 70 % of observed variations were attributable to the cumulative effects of atmospheric pressure, winds and steric variation. This annual signal was also detected by the GRACE mission at an amplitude of approximately 0.4 m; a comparison of the GRACE estimates with observations from a nearby tide gauge shows a correlation of 0.93, indicating that the GRGS (Groupe de Recherche en Géodesie Spatiale) GRACE solutions capture well the regional annual signal (Tregoning et al. 2008).

Using a nonlinear barotropic numerical model, Oliver and Thompson (2011) pointed out that the intraseasonal variations of the SSH field in the GOC are driven by surface wind stress variability related to the Madden–Julian Oscillation (MJO), while its low-frequency variability is propagated from the western equatorial Pacific, which is related to ENSO.

The studies mentioned above have provided a description of the annual cycle of SSH_{mass} and intraseasonal, interannual variations of the SSH in the GOC. However, aside from the work by Oliver and Thompson (2011), the interannual and decadal variability of SSH_{mass}, as well as its contribution to sea level change, have seldom been discussed. This study investigates variations in SSH in the GOC on interannual to decadal timescales by decomposing SSH into mass-induced and steric-related components, and explores their response to the ENSO and PDO via ocean processes.

This paper is structured as follows: the datasets used are described in Sect. 2, followed by the results in Sect. 3 on the variations in SSH on seasonal to decadal timescales. A discussion of the results and our conclusions are presented in Sect. 4.

2 Data and method

2.1 Global observations of SSH

SSH observations used in this study are based on a merged product from multiple satellite missions (T/P and ERS-1/2, followed by Jason-1/2 and Envisat) distributed on the Archiving, Validation, and Interpretation of Satellite Oceanographic (AVISO, http://www.aviso.oceanobs.com/) database system. Standard geophysical and environmental corrections, including ionosphere delay, dry and wet tropospheric corrections, electromagnetic bias, solid earth and ocean tides, ocean tide loading, pole tide, inverted barometer correction, sea state bias and instrumental corrections, have been applied (Le Traon et al. 1998; Le Traon and Ogor 1998). The product is available on a 1/3° Mercator grid at monthly intervals.

2.2 Global observations of SSH_{mass}

To estimate the mass component of the SSH budget, we use the monthly GRACE data (Release-04 solutions) produced by the Center for Space Research (CSR), University of Texas at Austin (http://grace.jpl.nasa.gov/data/mass/). The data, which is on a 1° × 1° spatial grid, is smoothed spatially using a 500-km Gaussian filter.

2.3 Global observations of SSH_{steric}

The monthly 1° × 1° gridded temperature and salinity dataset (Ishii et al. 2006) is used to calculate SSH_{steric} variations in the GOC. This data covers the period from 1945 to 2011 at a depth from the surface to 700 m.

2.4 Coastal observations of SSH

The presence of observed monthly SSH records at three tide stations (including Milner Bay, Karumba and Weipa; see their locations on Fig. 2) along the coast of Gulf of Carpentaria is from Permanent Service for Mean Sea Level (PSMSL) (http://www.psmsl.org/) (Holgate et al. 2013; PSMSL 2014). It provides an independent measure of the magnitude of the SSH variations against which the altimetry estimates can be validated.

2.5 Global observations of surface wind

For the global fields of zonal and meridional surface winds, we use data on a 0.25° × 0.25° grid obtained from the Environmental Research Division Data Access Program (ERDDAP) and the National Oceanic and Atmospheric Administration's National Climatic Data Center (NOAA/NCDC). The gridded data is generated from multiple satellite observations of the Department of Defense (DOD), NOAA, and the National Aeronautics and Space Administration (NASA), and wind retrievals of remote sensing systems (RSS), with monthly resolution from January 2003 to September 2011. To estimate the response of SSH to wind stress in the GOC, the local wind setup on

sea surface height (WSSH) was calculated following Oliver and Thompson (2010).

2.6 Eddy-resolving model

To reveal the decadal and long-term variability of SSH_{mass} and SSH, we used OFES [OGCM for the Earth Simulator] output. The OFES products (Masumoto et al. 2004; Sasaki et al. 2008) are based on the Modular Ocean Model version 3 (MOM3), with a near-global domain extending from 75°S to 75°N, but excluding the Arctic regions. Its horizontal resolution is 0.1°, and it has 54 vertical levels. In this study, hindcast simulation for the period 1955–2013 is used, with its daily atmospheric forcing from NCEP/NCAR Reanalysis data. When the multi-year average is removed, the variable sea surface height of OFES output is transformed into the model-based sea surface height (MSSH). Temperature and salinity outputs are used to calculate the OFES-based steric component ($MSSH_{steric}$). Thus the mass-induced term of the OFES version ($MSSH_{mass}$) is available when $MSSH_{steric}$ is subtracted from MSSH.

2.7 Data processing

The anomalies are obtained by subtracting the climatological monthly means and subsequently filtering out the intra-seasonal cycle using a 3-month running mean. The interannual components are the de-trended anomalies. Taking SSH as an example, the de-trended SSH anomalies are what we call interannual SSH. Similarly, the decadal components are the low-pass filtered (with a cutoff period at 7 years) anomalies. Study on the long-term variations of SSH, SSH_{mass}, SSH_{steric}, MSSH, $MSSH_{mass}$ and $MSSH_{steric}$ target the corresponding anomalies.

3 Results

3.1 Seasonal variability in SSH_{mass} over the GOC

Sea level records from tide gauges, altimetry observations and OFES output (Fig. 3) are quite well-matched in terms of amplitude and phase, suggesting that both altimetry

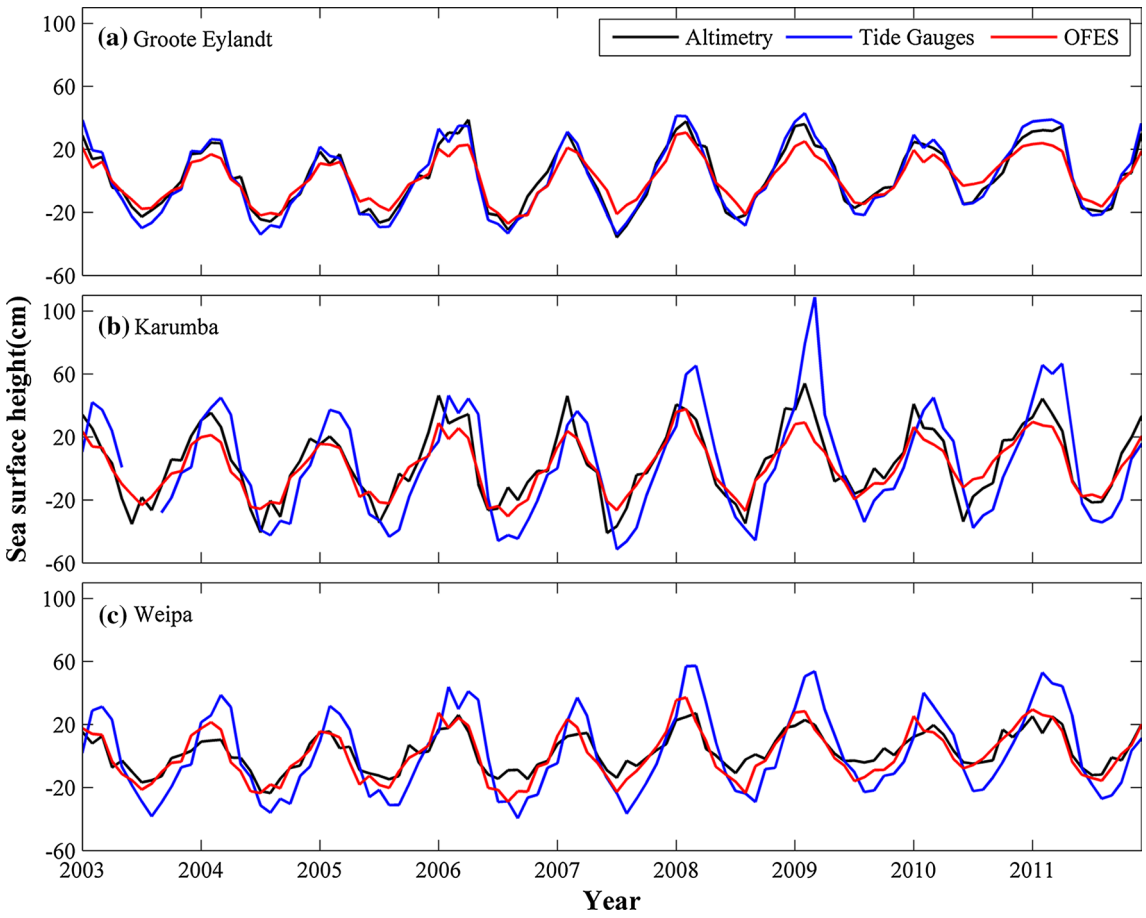

Fig. 3 Sea level records of altimetry (*black lines*), tide gauges (*blue lines*) and OFES (*red lines*) during the period 2003–2011 for (from *top* to *bottom*) Groote Eylandt, Karumba and Weipa

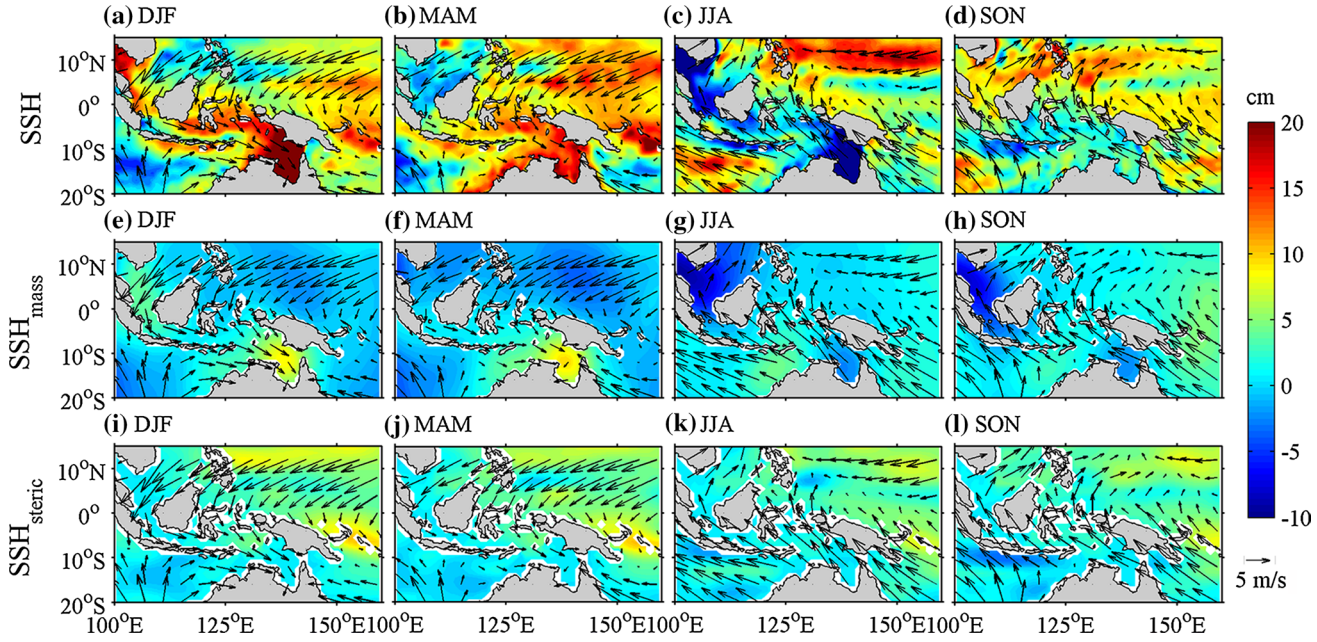

Fig. 4 Maps of seasonal mean SSH (**a**–**d**), SSH_{mass} (**e**–**h**) and SSH_{steric} (**i**–**l**) (cm, *shaded*), overlaid by climatological seasonal mean surface winds (m/s, vectors)

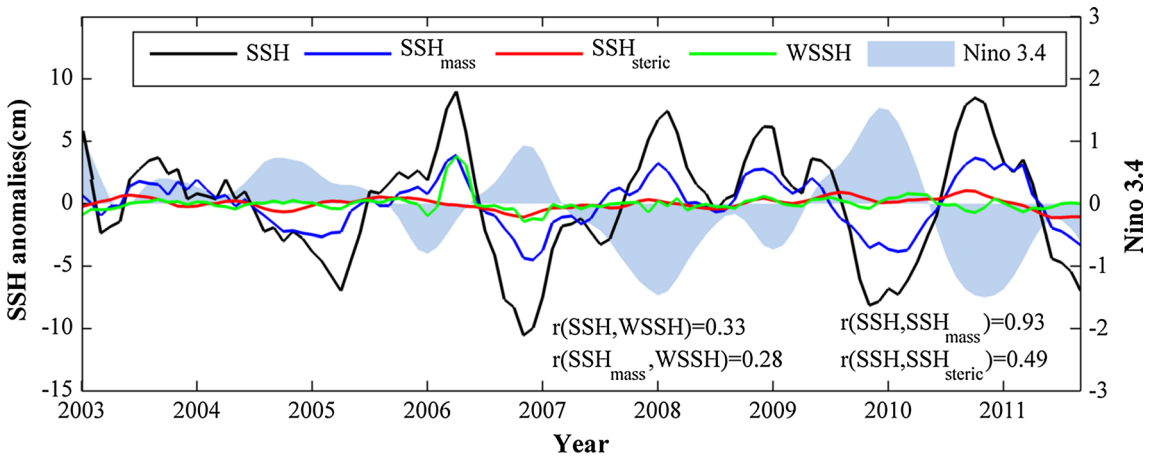

Fig. 5 Time series of interannual SSH (*black*), SSH_{steric} (*red*) and SSH_{mass} (*blue*), averaged over the area denoted by the *black box* in Fig. 2 (136°E–142°E, 18°S–8°S). The *green curve* and the *light blue shading* represent the local wind set-up on sea surface height (here denoted as WSSH) anomalies and the Niño 3.4 index, respectively

observations and OFES results effectively capture the SSH signal in the GOC.

The time series of SSH in the GOC shows significant seasonal variability (Fig. 3). Along with the southeasterly trade winds in austral winter, negative SSH_{mass} occupies the entire domain, while the northwesterly monsoon causes a significant rise in gulf-wide SSH_{mass} during the austral summer (Fig. 4). As it is dominated by SSH_{mass}, SSH exhibits a pattern that is similar to that of SSH_{mass}. It exerts strong seasonal variability which is attributable to the Ekman transport driven by the seasonally reversing monsoon. The same mechanism has been discussed for the western South China Sea (Cheng and Qi 2010), in agreement with Oliver and Thompson (2011), in which a good coherence between SSH variability and local wind variability is found on the seasonal timescale. Tregoning et al. (2008) carried out similar work using GRACE estimates over the period June 2002–May 2007. With better and longer-term GRACE observations, the climatological means in this study would be expected to be improved.

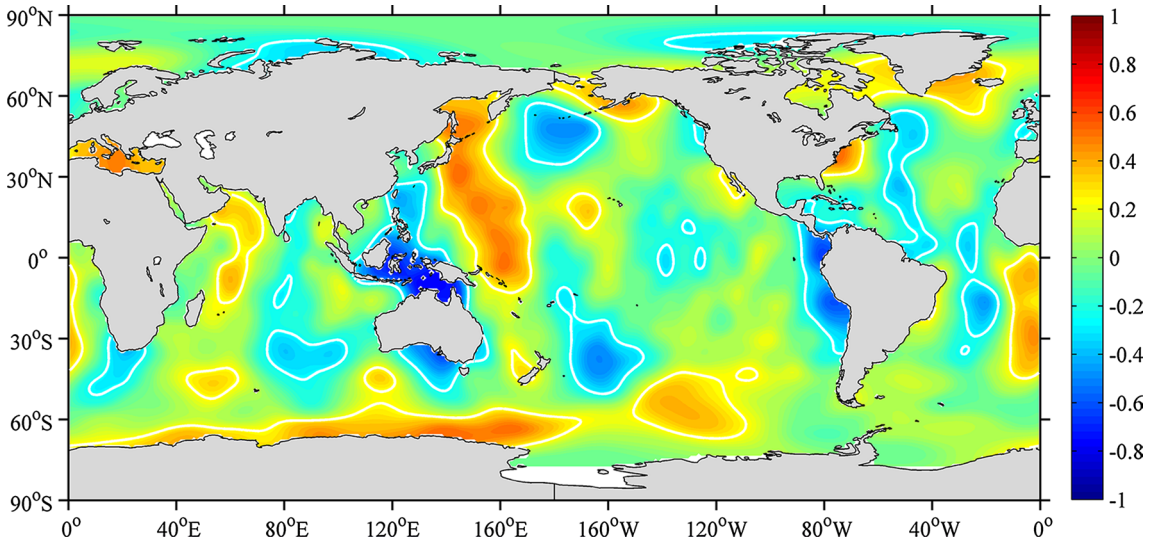

Fig. 6 Map of the correlation coefficient between interannual SSH_{mass} and Niño 3.4 index. *White contours* denote a 95 % confidence level

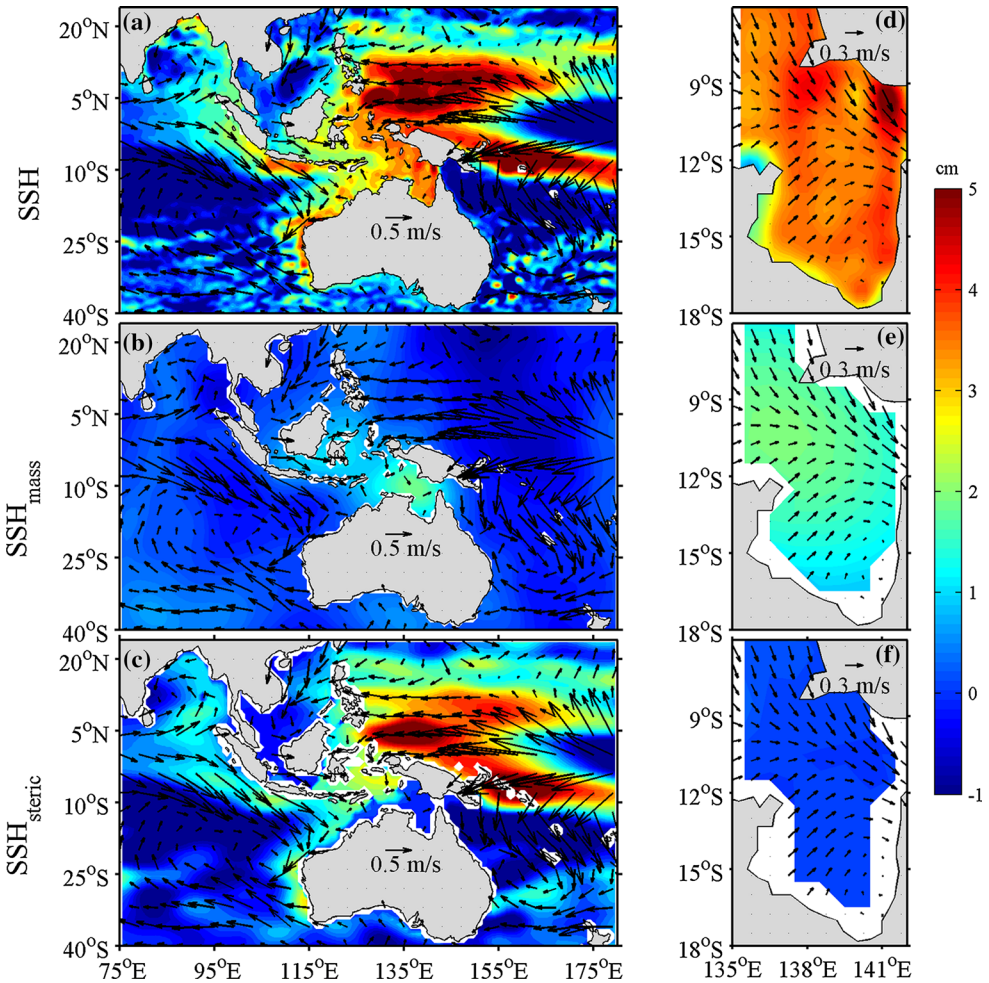

Fig. 7 Regression coefficients of interannual SSH (**a**, **d**), SSH_{mass} (**b**, **e**), SSH_{steric} (**c**, **f**) (cm, *shaded*) and NCDC 10-m winds (m/s, vectors) against the normalized negative Niño 3.4 index. *Right panels* are their corresponding values over the Gulf of Carpentaria

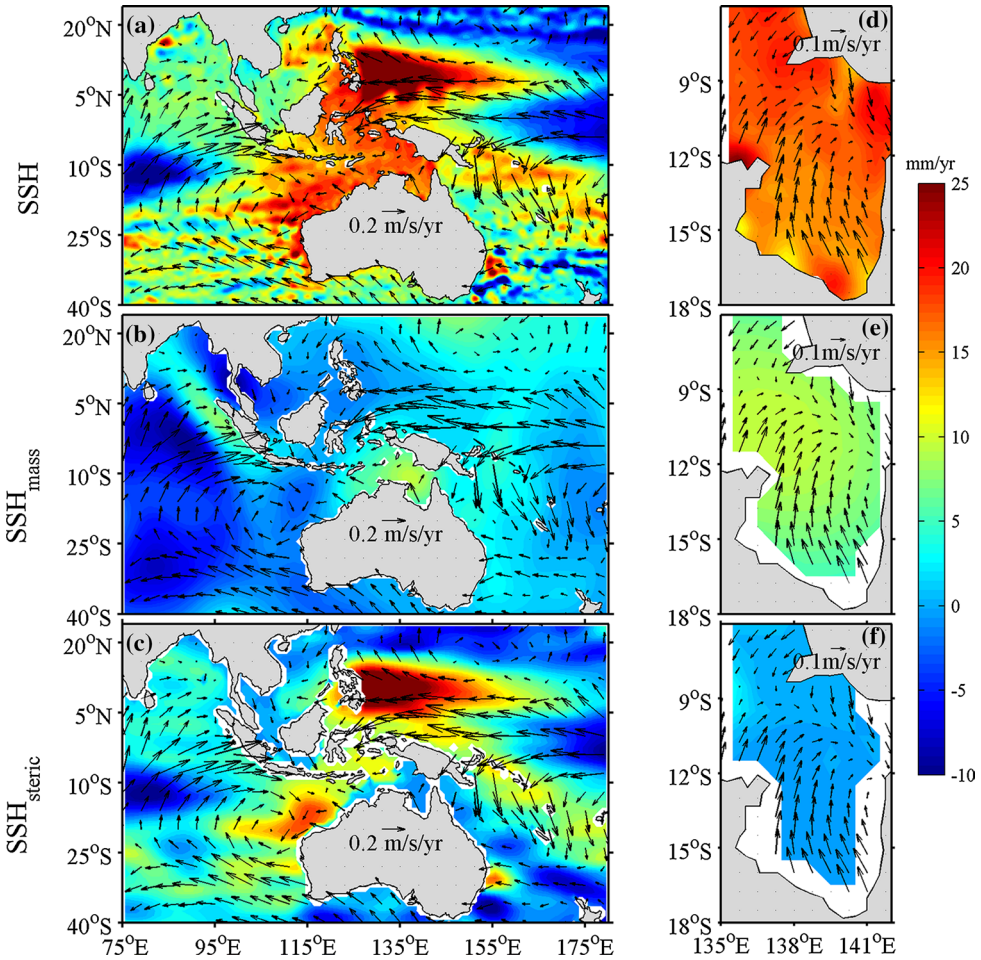

Fig. 8 Linear trends for SSH (**a**), SSH_{mass} (**b**) and SSH_{steric} (**c**) over the period 2003–2011 (mm/year, *shaded*), imposed on the linear trend of 10-m winds from NCDC/NOAA (m/s/year, vectors). *Right panels* are their corresponding values over the Gulf of Carpentaria

3.2 Interannual variations in gulf-wide SSH_{mass}

On an interannual timescale, the temporal evolution of gulf-mean SSH_{mass} matches well with that of observed SSH (Fig. 5, $r = 0.92$, significant at the 95 % confidence level), consistent with the results of Piecuch et al. (2013), who reported a significant interannual coherence between observed bottom pressure and SSH over shallow or semi-enclosed areas. However, the authors did not elucidate the reason for the good correlation or the cause of the interannual variability. In the Arafura Sea, just west of the region of interest in our study, interannual SSH and SSH_{mass} variations occur with a peak-to-peak amplitude of a few centimeters and periods of a couple of years (Piecuch et al. 2013). The correlation between the SSH_{steric} and SSH anomalies in the GOC is also significant (Fig. 5, $r = 0.47$, significant at 95 % confidence level), while the amplitude of SSH_{steric} is too weak to affect interannual SSH variability. Unlike seasonal variations, variation in local wind set-up on sea surface height (WSSH) is almost zero amplitude, with the exception of April 2006, when a severe tropical cyclonic hit the GOC. Neither SSH_{mass} nor SSH is significantly correlated with the WSSH, indicating that local wind cannot explain interannual variations in SSH_{mass} and SSH.

Recent studies have suggested that a significant portion of interannual sea level variation along the Australian coast originates from the western Pacific and is closely related to ENSO (Wijffels and Meyers 2004; Oliver and Thompson 2011). The curve denoting the temporal evolution of the Niño 3.4 index (sea surface temperature anomalies in 5°S–5°N, 170°–120°W, Fig. 5) is used to examine the relationship between SSH (including its two components) and ENSO. Three El Niño events (2004/2005, 2006/2007 and 2009/2010) and two La Niña events (2007/2008 and 2010/2011) took place during the study period. During the El Niño (La Niña) events, both SSH and SSH_{mass} experienced negative (positive) anomalies. Similar SSH variations were revealed in the waters surrounding Indonesia (Nerem et al. 1999) and along the southwestern coast of the Australian continent (Feng et al. 2004), where steric components dominate changes in SSH. Further analysis shows that both SSH and SSH_{mass} in the GOC are significantly correlated with the Niño 3.4 index (Fig. 5), with correlation coefficients of −0.71 and −0.75, respectively. Interestingly,

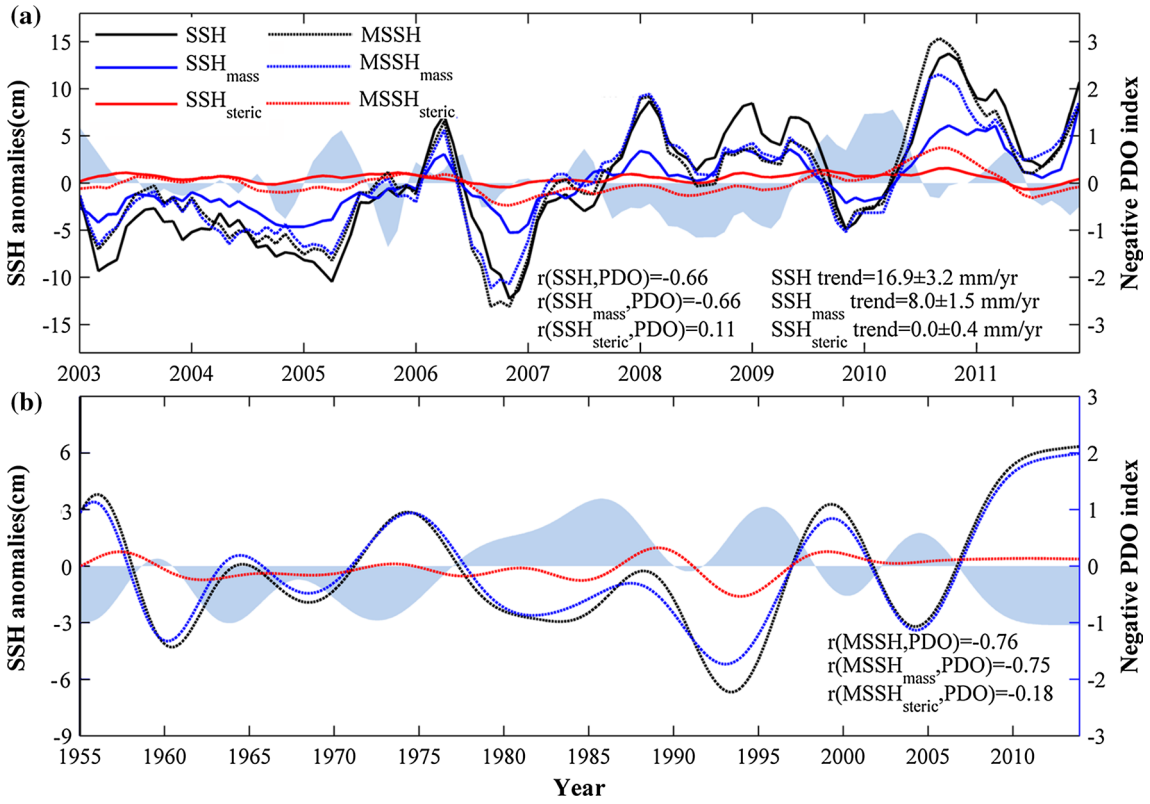

Fig. 9 **a** Time series of gulf-mean anomalies of SSH (*black*), SSH_{steric} (*red*) and SSH_{mass} (*blue*) averaged over the area denoted by the *black box* in Fig. 3 (136°E–142°E, 18°S–8°S). The *dotted curves* are the corresponding OFES estimates. **b** Time series of gulf-mean decadal MSSH (*black*), $MSSH_{steric}$ (*red*) and $MSSH_{mass}$ (*blue*). The *light blue shading* represents the negative PDO index (*right axis*)

the GOC is the very region where interannual SSH_{mass} is highly correlated to ENSO (Fig. 6). In the equatorial western Pacific, easterly (westerly) wind anomalies deepen (shoal) the thermocline during La Niña (El Niño) events, thereby increasing (decreasing) the steric component and, consequently, the total sea level. In contrast, the ENSO-related wind in the GOC leads to the divergence (convergence) of water during La Niña (El Niño) events (Fig. 7), which plays a negative role in variations of SSH and SSH_{mass}. Therefore, ENSO is expected to affect the interannual variability of SSH and SSH_{mass} via ocean processes.

3.3 Decadal and long-term variability in SSH_{mass}

In this section, we further identify the decadal and long-term variability in gulf-scale SSH_{mass} and SSH. Figure 8 shows long-term trends in SSH and SSH_{mass} in the GOC for 2003–2011, with maxima reaching ~20 mm/year for SSH and >8.0 mm/year for SSH_{mass}, whereas SSH_{steric} shows no significant trend. Gulf-mean SSH rises at a rate of 16.9 ± 3.2 mm/year. SSH_{mass} alone has a positive trend of 8.0 ± 1.5 mm/year, four times the rate of the rise in global SSH_{mass}, which was 2.0 mm/year during 2003–2012 (Johnson and Chambers 2013), while the linear trend of SSH_{steric} is not significant at a 95 % level (Fig. 9a). Significant correlation is found between SSH_{mass} and SSH ($r = 0.96$, significant at the 99 % level), whereas SSH_{steric} correlates to SSH at 0.34. The correlation coefficient between SSH and the sum of its two components is 0.96, indicating good agreement between SSH and its two components, and SSH_{mass} dominates the sea level change in terms of long-term variations in the GOC. The sum of SSH_{mass} and SSH_{steric} explain about half of the observed total sea level rise during 2003–2011. The discrepancy between the SSH and the sum of its two components may be due to uncertainties in the altimetry and GRACE data and subsurface temperature and salinity analyses. The GRACE data has a relatively low signal-to-noise ratio in the tropics (Wahr et al. 2004) and greatly underestimates the SSH_{mass} in the GOC. Quinn and Ponte (2010) noted uncertainty in ocean mass trends of up to ~2.5 mm/year over 2003–2008 from GRACE observations.

Surface winds can be used to explain SSH_{mass} in the Southern Ocean (Boening et al. 2011) and the northwestern North Pacific (Cheng et al. 2013). However, atmospheric circulation during this period in the GOC had a cyclonic trend (Fig. 8), which cannot explain the rise in SSH_{mass} over the region, suggesting that other processes are responsible for the rise in sea level in the basin.

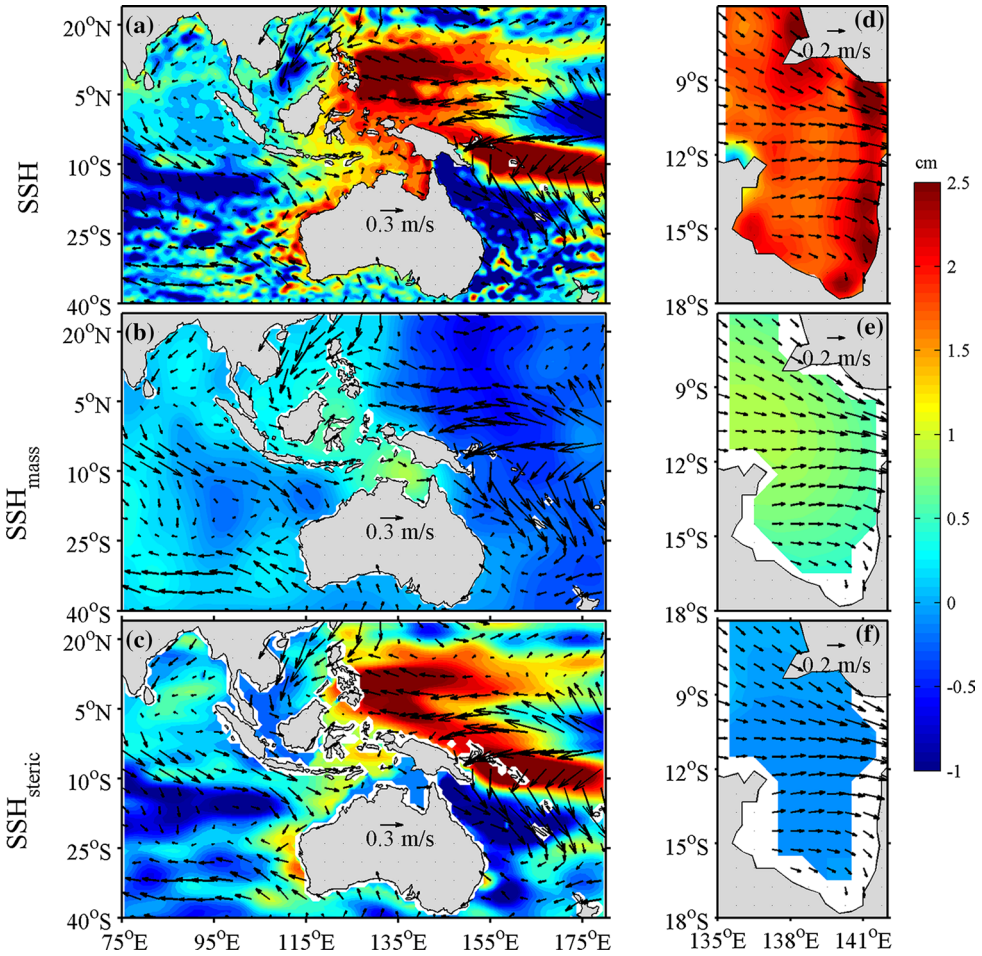

Fig. 10 Regression coefficients of SSH anomalies (**a**, **d**), SSH_{mass} anomalies (**b**, **e**), SSH_{steric} anomalies (**c**, **f**) (cm, *shaded*) and NCDC 10-m wind anomalies (m/s, vectors) against the normalized negative PDO index

Recent studies have indicated that the PDO accounts for a significant portion of SSH inter-decadal variability and decadal trends in the western equatorial Pacific (Bromirski et al. 2011; Merrifield et al. 2012). In the GOC, just east of the Arafura Sea, the decadal trend may be affected by the PDO. Assuming that the PDO does affect the decadal trend in the GOC, the above-mentioned long-term linear trends may be partly due to large-scale climate modes in the ocean–atmosphere system. Therefore, it is necessary to assess the decadal variability in SSH and SSH_{mass}, which is helpful for isolating the contribution of climate modes to the rise in sea level over the last decade.

Figure 9a shows that both gulf-mean SSH and SSH_{mass} closely correlate with the PDO ($r = -0.66$), while the correlation between SSH_{steric} and PDO is not significant ($r = 0.11$). Since the GRACE data is not of adequate length to explore the relationship between lower-frequency variability of SSH and the PDO, we use the OFES model output. This model covers a longer period and provides a good reproduction of the gulf-scale long-term SSH variations (including the total and its two components) (Fig. 9a). The MSSH, $MSSH_{mass}$ and $MSSH_{steric}$ correlate to their corresponding observations at 0.95, 0.92 and 0.74. Moreover, the sea level budget in the OPES model is closed, unlike in the observations. The MSSH maintains a rising trend of 13.8 ± 3.4 mm/year over 2003–2011, with 12.8 ± 2.9 mm/year and 1.1 ± 0.9 mm/year for the $MSSH_{mass}$ and $MSSH_{steric}$, respectively. The model-derived linear trend is ~3 mm/year less than that of the altimetry observations, which is approximately the rate of the rise in global mean SSH_{mass} due to ice melting (Johnson and Chambers 2013), and this component is not taken into account in the OFES. In the model, mass-induced sea level variations dominate total sea level change in terms of long-term variations.

On a decadal timescale, gulf-mean MSSH and $MSSH_{mass}$ fell during 1955–1968, and then rose until 1975, reaching a high level. They then fell again, reaching the lowest level in 1993, and then rose rapidly over the last two decades. Between 1955 and 2013, the decadal MSSH and $MSSH_{mass}$ from the OFES model correlate to the PDO at −0.76 and −0.75, respectively (Fig. 9b). The good correlations between sea level and the PDO indicate that decadal variability of MSSH and $MSSH_{mass}$ may be modulated by

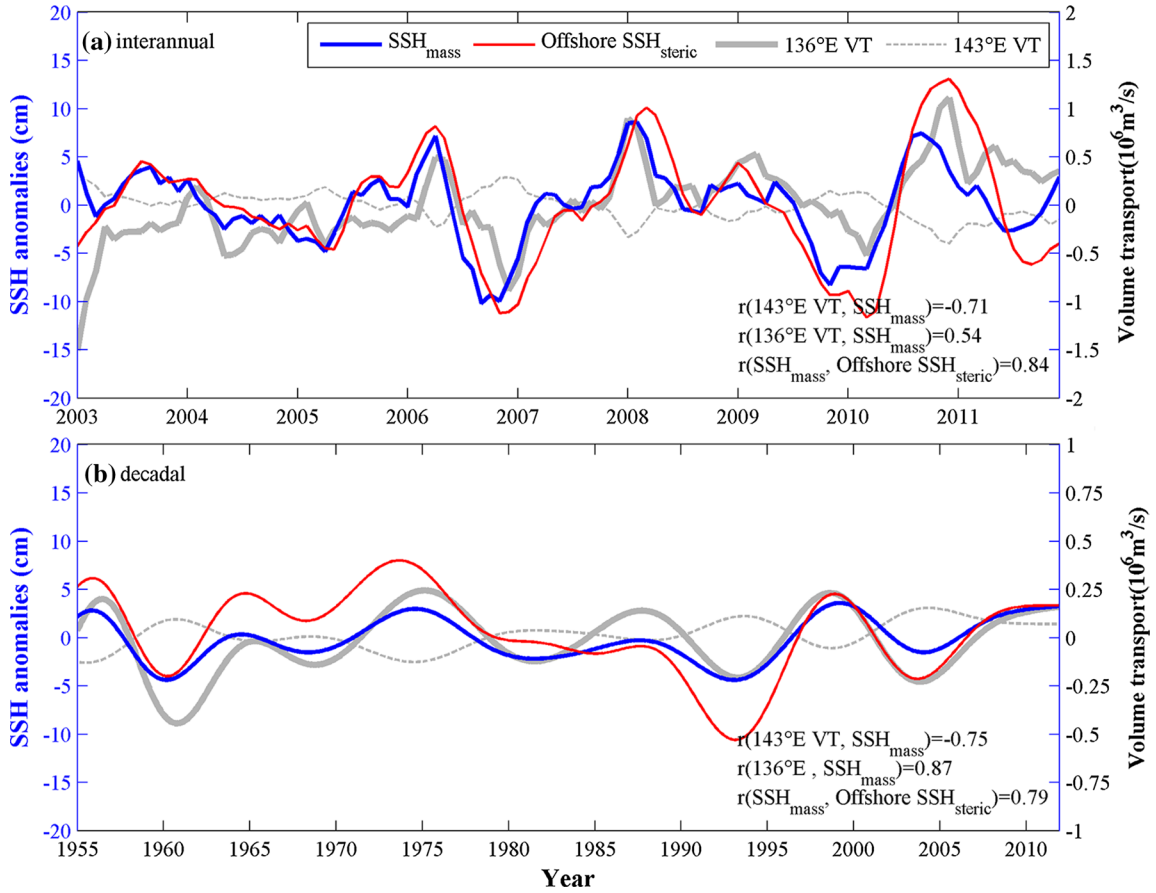

Fig. 11 **a** Interannual component of the basin-wide $MSSH_{mass}$ (*blue*), offshore $MSSH_{steric}$ (*red*) averaged over the area in the *red box* in Fig. 2 (130°E–133°E, 7°S–3°S), and the volume transport (denoted as VT) at 136°E (*solid gray line*) and 143°E (*dashed gray line*) calculated from OFES zonal and meridional velocity. **b** The same as (**a**) but for the decadal component

the PDO, which can affect the sea level trend over a relative short period. Similar to interannual variations, the PDO-related wind, exhibiting a cyclonic pattern (Fig. 10), leads to divergence, and consequently drives a drop in sea level. This it cannot explain the decadal and long-term variability of SSH_{mass} and SSH. Which mechanism related to the PDO, then, can explain the high rising rate of the SSH_{mass} (SSH) in the GOC?

3.4 Origin of low-frequency variability in SSH_{mass}

Previous studies have shown that westward equatorial Rossby waves, excited by trade wind variations, can propagate through the Ombai Strait and then poleward northwesterly to the western Australian coast as coastal-trapped waves (Meyers 1996; Holgate and Woodworth 2004; Wijffels and Meyers 2004). These waves transmit fluctuations in the thermocline and thus lead to SSH_{steric} variations along their paths. The equatorial easterly anomalies exhibit an intensified pattern. Note that in this case, the SSH_{steric} variations do maintain a high rising rate of about 15.0 mm/year, the same magnitude as altimetry observations just to the west in the shallow waters of the Arafura Sea, Timor Sea and GOC (See Fig. 8) in this given atmospheric context. Landerer et al. (2007) demonstrated that net mass transfers could occur between shallow and deep zones as a result of steric changes in the ocean. In other words, the high positive SSH_{steric} anomalies west of the GOC could lead to a sharp pressure gradient between deep regions and the nearby shallow waters. The difference could push the flow of water from deep into shallow regions, resulting in a mass gain in the GOC and a mass loss in the adjacent deep waters. This joint theory can also explain the interannual variations in SSH_{mass}, in which stronger equatorial easterly anomalies lead to higher SSH_{mass} (SSH) during the negative ENSO phase (see Fig. 7), and vice versa.

To quantitatively test this hypothesis, we first compared the gulf-mean $MSSH_{mass}$ against the offshore $MSSH_{steric}$ (represented by the value averaged over 130°E–133°E and 7°S–3°S, just right in the wave path and northwest of the GOC, the *red box* in Fig. 2). Secondly, we calculated the volume transport into and out of the GOC using the rough

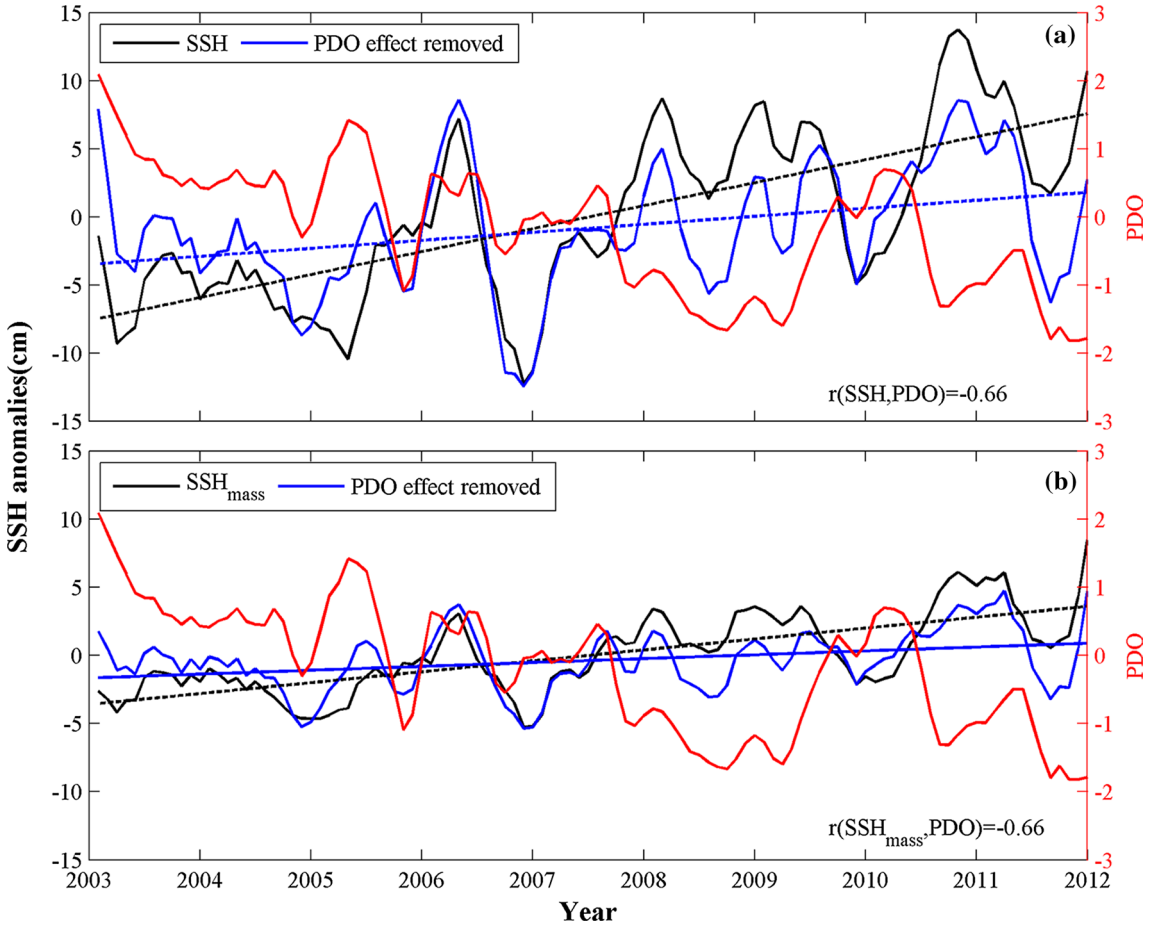

Fig. 12 **a** Time series of the basin-wide SSH anomalies (*solid black*), and the residual with the PDO effect removed (*solid blue*), with the corresponding *dashed lines* representing the linear trends. **b** The same as (**a**) for SSH_{mass}

estimate of the 136°E section (denoted by 136°E VT). On an interannual timescale, $MSSH_{mass}$ correlates significantly with the offshore $MSSH_{steric}$, at 0.84. The good correlation implies that the offshore $MSSH_{steric}$ along the wave path may affect the $MSSH_{mass}$. On such a timescale, therefore, the rough volume transport into and out of the GOC varies almost in phase with the gulf-mean $MSSH_{mass}$, with a correlation coefficient of 0.54 (Fig. 11a). The $MSSH_{mass}$ is further compared against the volume transport at the 143°E section (denoted by the 143°E VT), with the latter representing the water exchange between the GOC and the South Pacific. On an interannual timescale, the amplitude of the 143°E VT is smaller than that at 136°E. The former has a negative contribution to the gulf-mean $MSSH_{mass}$ variations and varies out of phase with $MSSH_{mass}$. These results suggest that the hypothesis is accurate for interannual variations. Similarly, it holds true on the decadal timescale: firstly, the correlation between $MSSH_{mass}$ and $MSSH_{steric}$ was 0.79 and between $MSSH_{mass}$ and 136°E VT was 0.87; secondly, the water exchange between the GOC and the South Pacific shows an out-of-phase relationship with $MSSH_{mass}$ (Fig. 11b).

4 Conclusions and discussion

In this study, a dome-like rising trend in SSH_{mass} anomalies in the GOC was revealed by GRACE estimates. In conjunction with satellite altimetry and steric budget derived from subsurface temperature and salinity analyses, mass-induced sea level variations in the GOC on multiple timescales were investigated. Seasonal gulf-scale variations in SSH can be attributed to SSH_{mass} variations and local winds acting as the dynamic driver. With regard to interannual and long-term variations, the pattern of SSH_{mass} variability resembles that of SSH, and is related to large-scale climate modes including ENSO and PDO. The local wind anomalies associated with ENSO and PDO cannot explain such low-frequency variability in SSH_{mass}. Oceanic waves propagating from the western Pacific cause changes in SSH_{steric} west of the Arafura Sea and the GOC, resulting in a sharp pressure gradient between deep regions and the GOC, which drives an exchange of water mass.

The observed mean sea level in the GOC was significantly correlated with the PDO over the period 2003–2011

($r = -0.66$), indicating that linear sea level trends over the past 9 years may have been greatly affected by low-frequency variability associated with the PDO. To what extent, then, can the PDO explain the rise in SSH in the GOC during the period 2003–2011? Multivariable linear regression (MVLR) analysis is used here to determine the contribution of the PDO (Zhang and Church 2012), which returns two values: one is the pure linear trend and the other is the linear trend associated with the PDO. Results show that the contribution of the PDO to the gulf-scale SSH (SSH_{mass}) trend was approximately 11.0 mm/year (5.0 mm/year) in 2003–2011. After removing the trend associated with the PDO, the linear trends for SSH and SSH_{mass} drop to 5.9 ± 3.3 and 2.8 ± 1.5 mm/year, respectively (Fig. 12). The PDO appears to account for about 65 % of the sea level rise in the GOC during 2003–2011. Thus, a portion of the rise in SSH is the regional sea adjustment to the PDO phase shift.

Acknowledgments This work was supported by the Strategic Priority Research Program of the Chinese Academy of Sciences (grant numbers XDA11010103 and XDA11010203) and the Natural Science Foundation of China (41176023, 41276108). X.H.C is also sponsored by the "Youth Innovation Promotion Association", CAS (SQ201204, LTOZZ1202) and the China Scholarship Council. The OFES simulation was conducted on the Earth Simulator under the support of JAMSTEC.

References

Boening C, Lee T, Zlotnicki V (2011) A record-high ocean bottom pressure in the South Pacific observed by GRACE. Geophys Res Lett 38(4):L04602

Bromirski PD, Miller AJ, Flick RE, Auad G (2011) Dynamical suppression of sea level rise along the Pacific coast of North America: indications for imminent acceleration. J Geophys Res 116(C7):C07005

Calafat FM, Marcos M, Gomis D (2010) Mass contribution to Mediterranean Sea level variability for the period 1948–2000. Glob Planet Chang 73(3–4):193–201

Carton JA, Giese BS, Grodsky SA (2005) Sea level rise and the warming of the oceans in the Simple Ocean Data Assimilation (SODA) ocean reanalysis. J Geophys Res 110(C9):C09006

Cazenave A, Nerem RS (2004) Present-day sea level change: observations and causes. Rev Geophys 42:RG3001. doi:10.1029/2003RG000139

Chambers DP (2006) Observing seasonal steric sea level variations with GRACE and satellite altimetry. J Geophys Res 111(C3):C03010

Cheng X, Qi Y (2010) On steric and mass-induced contributions to the annual sea-level variations in the South China Sea. Glob Planet Chang 72(3):227–233

Cheng X, Li L, Du Y, Wang J, Huang R-X (2013) Mass-induced sea level change in the northwestern North Pacific and its contribution to total sea level change. Geophys Res Lett 40(15):3975–3980

Feng M, Li Y, Meyers G (2004) Multidecadal variations of Fremantle sea level: footprint of climate variability in the tropical Pacific. Geophys Res Lett 31(16):L16302

Forbes A, Church J (1983) Circulation in the Gulf of Carpentaria. II. Residual currents and mean sea level. Aust J Mar Freshw Res 34(1):11–22

García D, Chao BF, Del Río J, Vigo I, García-Lafuente J (2006) On the steric and mass-induced contributions to the annual sea level variations in the Mediterranean Sea. J Geophys Res 111(C9):C09030

Harris PT (2007) Applications of geophysical information to the design of a representative system of marine protected areas in southeastern Australia. In: Todd BJ, Greene HG (eds) Mapping the seafloor for habitat characterisation, vol 47. Geoscience Australia, Canberra, pp 449–468

Holgate SJ, Woodworth PL (2004) Evidence for enhanced coastal sea level rise during the 1990s. Geophys Res Lett 31(7):L07305

Holgate Simon J, Matthews Andrew, Woodworth Philip L, Rickards Lesley J, Tamisiea Mark E, Bradshaw Elizabeth, Foden Peter R, Gordon Kathleen M, Jevrejeva Svetlana, Pugh Jeff (2013) New data systems and products at the permanent service for mean sea level. J Coast Res 29(3):493–504. doi:10.2112/JCOASTRES-D-12-00175.1

Ishii M, Kimoto M, Sakamoto K, Iwasaki S-I (2006) Steric sea level changes estimated from historical ocean subsurface temperature and salinity analyses. J Oceanogr 62(2):155–170

Johnson GC, Chambers DP (2013) Ocean bottom pressure seasonal cycles and decadal trends from GRACE Release-05: ocean circulation implications. J Geophys Res 118(9):4228–4240

Landerer FW, Jungclaus JH, Marotzke J (2007) Ocean bottom pressure changes lead to a decreasing length-of-day in a warming climate. Geophys Res Lett 34(6):L06307

Le Traon PY, Ogor F (1998) ERS-1/2 orbit improvement using TOPEX/POSEIDON: the 2 cm challenge. J Geophys Res 103(C4):8045

Le Traon PY, Nadal F, Ducet N (1998) An improved mapping method of multisatellite altimeter data. J Atmos Ocean Technol 15:522–534

Masumoto Y, Sasaki H, Kagimoto T, Komori N, Ishida A, Sasai Y, Miyama T, Motoi T, Mitsudera H, Takahashi K, Sakuma H, Yamagata T (2004) A fifty-year eddy-resolving simulation of the world ocean—preliminary outcomes of OFES (OGCM for the Earth Simulator). J Earth Sim 1:35–56

McLoughlin K (2004) Northern prawn fishery. In: Canton A, McLoughlin K (eds) Fishery Status Reports 2004: Status of fish stocks managed by the Australian Government. Bureau of Rural Sciences, Canberra, pp 25–36

Merrifield MA, Thompson PR, Lander M (2012) Multidecadal sea level anomalies and trends in the western tropical Pacific. Geophys Res Lett 39(13):L13602

Meyers G (1996) Variation of Indonesian throughflow and the El Niño-Southern Oscillation. J Geophys Res 101(C5):12255–12263

Nerem RS, Chambers DP, Leuliette EW, Mitchum GT, Giese BS (1999) Variations in global mean sea level associated with the 1997–1998 ENSO event: implications for measuring long term sea level change. Geophys Res Lett 26(19):3005–3008

Nerem R, Wahr J, Leuliette E (2003) Measuring the distribution of ocean mass using GRACE. Space Sci Rev 108(1–2):331–344

Nicholls RJ (2011) Planning for the impacts of sea level rise. Oceanogr 24(2):144–157. doi:10.5670/oceanog.2011.34

Oliver ECJ, Thompson KR (2010) Madden-Julian Oscillation and sea level: local and remote forcing. J Geophys Res 115(C1):C01003

Oliver ECJ, Thompson KR (2011) Sea level and circulation variability of the Gulf of Carpentaria: influence of the Madden-Julian Oscillation and the adjacent deep ocean. J Geophys Res 116(C2):C02019

Permanent Service for Mean Sea Level (PSMSL) (2014) "Tide Gauge Data", Retrieved 17 Nov 2014 from http://www.psmsl.org/data/obtaining/

Piecuch CG, Quinn KJ, Ponte RM (2013) Satellite-derived interannual ocean bottom pressure variability and its relation to sea level. Geophys Res Lett 40(12):3106–3110

Quinn KJ, Ponte RM (2010) Uncertainty in ocean mass trends from GRACE. Geophys J Int 181:762–768. doi:10.1111/j.1365-246X.04508.x

Sasaki H, Nonaka M, Masumoto Y, Sasai Y, Uehara H, Sakuma H (2008) An eddy-resolving hindcast simulation of the quasiglobal ocean from 1950 to 2003 on the Earth Simulator. In: Hamilton K, Ohfuchi W (eds) High Resolution Numerical Modelling of the Atmosphere and Ocean, chapter 10. Springer, New York, pp 157–185

Tregoning P, Lambeck K, Ramillien G (2008) GRACE estimates of sea surface height anomalies in the Gulf of Carpentaria, Australia. Earth Planet Sci Lett 271(1–4):241–244

Wahr J, Swenson S, Zlotnicki V, Velicogna I (2004) Time-variable gravity from GRACE: first results. Geophys Res Lett 31(11):L11501

Wijffels S, Meyers G (2004) An intersection of oceanic waveguides: variability in the Indonesian Throughflow region. J Phys Oceanogr 34(5):1232–1253

Wouters B, Chambers D (2010) Analysis of seasonal ocean bottom pressure variability in the Gulf of Thailand from GRACE. Glob Planet Chang 74(2):76–81

Zhang X, Church JA (2012) Sea level trends, interannual and decadal variability in the Pacific Ocean. Geophys Res Lett 39(21):L21701